Parallel Higher Order DGTD and FETD for Transient Electromagnetic-Circuital-Thermal Co-Simulation

Huan Huan Zhang, *Member, IEEE*, Pan Pan Wang, Li Jun Jiang, *Fellow, IEEE*, Wei E. I. Sha, *Senior Member, IEEE*, Mei Song Tong, *Senior Member, IEEE*, Ying Liu, *Senior Member, IEEE*, Wei Jun Wu, and Guang Ming Shi, *Fellow, IEEE*

***Abstract*— A hybrid higher order discontinuous Galerkin time-domain (DGTD) method and finite-element time-domain (FETD) method with parallel technique is proposed for electromagnetic (EM)–circuital–thermal co-simulation in this article. For electromagnetic simulation, DGTD method with higher order hierarchical vector basis functions is used to solve Maxwell equation. Circuit simulation is carried out by modified nodal analysis method. For thermal simulation, FETD method with higher order interpolation scalar basis functions is adopted to solve heat conduction equation. To implement electromagnetic–circuital–thermal co-simulation, the electromagnetic and circuital equations are strongly coupled through voltages, currents, and electric fields at the lumped ports first. Then the electromagnetic and thermal equations are weakly coupled with electromagnetic loss and temperature-dependent medium parameters. Finally, large-scale parallel technique is used to accelerate the process of multiphysics simulation. Numerical results are given to validate the correctness and capability of the proposed electromagnetic–circuital–thermal co-simulation method.**

***Index Terms*— Discontinuous Galerkin time-domain (DGTD) method, electromagnetic (EM)–circuital–thermal co-simulation, finite-element time-domain (FETD) method, higher order basis functions, parallel technique.**

I. Introduction

THE electromagnetic (EM) field–circuit coupling and thermal management problems are more and more serious with the increase in working frequency and power in microwave circuits. The accuracy of traditional pure circuit simulation cannot meet the engineering requirements with the increase in frequency. Numerical simulation method of electromagnetic field and traditional circuit theory must cooperate to implement electromagnetic–circuital co-simulation. Moreover, the large heat flux induced by high power can result in high temperature and nonuniform stress in microwave circuits. Thus, circuit malfunction will naturally happen over the long term. Therefore, electromagnetic–thermal co-simulation is significant in the initial design stage of microwave circuits. If we consider the influences of both high working frequency and high power, the electromagnetic field, lumped circuit, and thermal field will couple together and interact with each other. Electromagnetic–circuital–thermal co-simulation is indispensable under such circumstances.

Many scholars have focused on the electromagnetic–circuital co-simulation method and electromagnetic–thermal co-simulation method. Electromagnetic–circuital co-simulation method consists of electromagnetic simulation method and circuit simulation method, which are linked together by voltages, currents, and electromagnetic fields at the lumped ports. The studies in this area are mainly related to different electromagnetic and circuital simulation methods. For instance, the finite-difference time-domain (FDTD) method [1]–[3], finite-element time-domain (FETD) method [4]–[6], time-domain integral equation (TDIE) method [7], [8], and the discontinuous Galerkin time domain (DGTD) method [9], [10] are used for electromagnetic simulation. Modified nodal analysis method [2], [4], [7], [9], scattering matrices method [6], and behavioral macromodel method [3], [8], [10] are applied for circuit simulation. The electromagnetic–thermal co-simulation method is composed of electromagnetic simulation method and thermal simulation method, which are mutually coupled through electromagnetic loss and constitutive parameter. The studies on electromagnetic–thermal co-simulation method are relatively less compared with the electromagnetic–circuital co-simulation method. Much emphasis is put on numerical methods for solution of differential equations including Maxwell equation and heat conduction equation. The FDTD method [12], [13], FEM [13], [14], DGTD method [15], and spectral-element time-domain (SETD) method [16] are

Manuscript received December 24, 2021; accepted March 2, 2022. Date of publication April 20, 2022; date of current version June 3, 2022. This work was supported in part by the National Natural Science Foundation of China under Grant 62127812 and Grant 61701376; and in part by the Joint Foundation of Key Laboratory of Shanghai Jiao Tong University-Xidian University, Ministry of Education, under Grant LHJJ/2020-03. *(Corresponding author: Ying Liu.)*

Huan Huan Zhang, Pan Pan Wang, and Ying Liu are with the National Key Laboratory of Antennas and Microwave Technology, Xidian University, Xi'an 710071, China (e-mail: hhzhang@xidian.edu.cn; liuying@mail.xidian.edu.cn).

Li Jun Jiang is with the Department of Electrical and Electronic Engineering, The University of Hong Kong, Hong Kong.

Wei E. I. Sha is with the College of Information Science and Electronic Engineering, Zhejiang University, Hangzhou 310058, China.

Mei Song Tong is with the College of Electronics and Information Engineering, Tongji University, Shanghai 201804, China.

Wei Jun Wu is with the Science and Technology on Electromagnetic Compatibility Laboratory, China Ship Development and Design Center, Wuhan 430064, China.

Guang Ming Shi is with the School of Artificial Intelligence, Xidian University, Xi'an 710071, China.

Color versions of one or more figures in this article are available at https://doi.org/10.1109/TMTT.2022.3164703.

Digital Object Identifier 10.1109/TMTT.2022.3164703

adopted for electromagnetic–thermal co-simulation. It is worth mentioning that the electromagnetic simulation is carried out in the frequency domain in [13] and [14] with the hypothesis that time-harmonic excitation sources are imposed. Obviously, it is not applicable when a transient excitation source like a pulse is applied when two-way coupling of EM and thermal is considered. Another issue of concern is that the simultaneous simulation of electromagnetic, circuit, and thermal, has not been found yet in the existing literatures [16]. However, electromagnetic–circuital–thermal coupling is a very common phenomenon in microwave circuits [18]–[21]. For instance, the operating frequency and integration density are increased rapidly in present high-speed integrated circuits (ICs). The electromagnetic field effects such as crosstalk, radiation of the interconnects, and its coupling with the package become more and more noticeable. So classical circuit simulation must be replaced by electromagnetic–circuital co-simulation with the consideration of simulation accuracy. Meanwhile, the performance of IC is sensitive to temperature variations, which has influences on the material properties of ICs. So the electromagnetic–thermal interactions must also be taken into account simultaneously.

In this work, we propose a hybrid higher order DGTD and FETD method with parallel technique for transient electromagnetic–circuital–thermal co-simulation. The DGTD method with higher order hierarchical vector basis functions is used for electromagnetic simulation. The modified nodal analysis method is adopted for circuit simulation. The FETD method with higher order interpolation scalar basis functions is used for thermal simulation. Then the electromagnetic, circuit, and thermal simulations are coupled together by a well-designed coupling mechanism. Finally, large-scale parallel technique is applied to accelerate the process of multiphysics simulation. The contribution of this work includes: 1) simultaneous simulation of electromagnetic, circuit, and thermal is implemented; 2) higher order basis function technique is applied for multiphysics simulation to improve the simulation accuracy and efficiency; and 3) large-scale parallel technique is adopted to accelerate the multiphysics simulation process. In summary, a systematic solution for accurate and efficient electromagnetic–circuital–thermal co-simulation of microwave circuits is provided in this article.

This article is organized as follows. In Section II, the theories and formulations of the proposed method are introduced. In Section III, numerical examples are provided to present the accuracy, efficiency, and capability of the proposed method. Ultimately, conclusions are drawn in Section IV.

II. Theories and Formulations

Fig. 1 shows the flowchart of electromagnetic-circuital–thermal co-simulation. At the ith time step, the electromagnetic–circuital co-simulation is carried out first since the rate of change in voltages, currents, and electromagnetic fields is at the same level. After that, the power loss of the material can be calculated according to the electromagnetic field inside the material, which serves as the heat sources of thermal simulation. After thermal simulation at the ith time step, the computation process will terminate if i equals to the predetermined total number of time steps N_t. Otherwise, temperature-dependent constitutive parameters such as permittivities, permeabilities, and conductivities of materials are updated. It is worth mentioning that only temperature-dependent conductivities of materials are considered while the permittivities and permeabilities are assumed to be constant for the sake of simplicity. But the proposed method is also applicable to materials with temperature-dependent permittivities and permeabilities. The electromagnetic–circuital co-simulation at next time step continues. In the following, we will present the technical details of the simulation process.

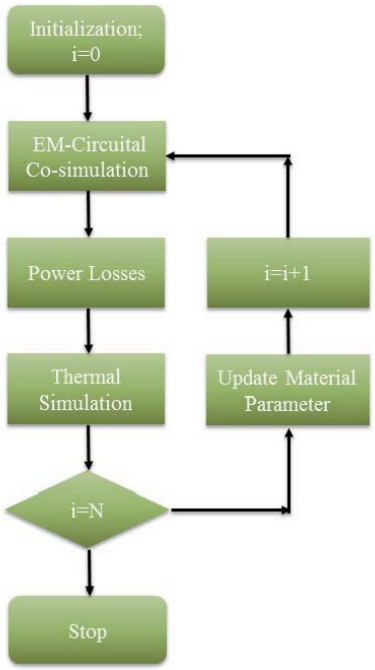

Fig. 1. Flowchart of electromagnetic–circuital–thermal co-simulation.

A. Electromagnetic–Circuital Co-Simulation With Higher Order DGTD Method

The EM simulation starts from the Maxwell curl equations

$$\varepsilon \frac{\partial \mathbf{E}}{\partial t} = \nabla \times \mathbf{H} - \sigma \mathbf{E} \tag{1}$$

$$\mu \frac{\partial \mathbf{H}}{\partial t} = -\nabla \times \mathbf{E} \tag{2}$$

with permittivity ε, permeability μ and conductivity σ.

Let V be the computational domain where the DGTD method is applied for EM simulation. The domain V is subdivided into N tetrahedron elements $V_1, V_2, \ldots, V_N$. The boundary of V_i is ∂V_i. The second-order hierarchical vector

basis function defined in V_i is $\mathbf{N}_k$ [22], [23]

$$\mathbf{N}_k = L_{k1}\nabla L_{k2} - L_{k2}\nabla L_{k1} \quad (k = 1, 2, \ldots, 6) \tag{3}$$
$$\mathbf{N}_k = L_{k1}\nabla L_{k2} + L_{k2}\nabla L_{k1} \quad (k = 7, 8, \ldots, 12) \tag{4}$$
$$\mathbf{N}_k = L_{k3}(L_{k1}\nabla L_{k2} - L_{k2}\nabla L_{k1}) \quad (k = 13, 14, \ldots, 16) \tag{5}$$
$$\mathbf{N}_k = L_{k1}(L_{k3}\nabla L_{k2} - L_{k2}\nabla L_{k3}) \quad (k = 17, 18, \ldots, 20) \tag{6}$$

where $\mathbf{N}_k (k = 1, 2, \ldots, 6)$ are the first-order basis functions. $k1, k2, k3$ denote the three nodes of the tetrahedral surface, and L refers to the volume coordinate.

Using the Galerkin testing method to (1) and (2), we can obtain

$$\int_{V_i} \varepsilon \mathbf{N}_k \cdot \frac{\partial \mathbf{E}}{\partial t} dV + \int_{V_i} \mathbf{N}_k \cdot \sigma \mathbf{E} dV = \int_{V_i} \nabla \times \mathbf{N}_k \cdot \mathbf{H} dV + \int_{\partial V_i} \mathbf{N}_k \cdot \hat{n} \times \mathbf{H} dS \tag{7}$$

$$\int_{V_i} \mu \mathbf{N}_k \cdot \frac{\partial \mathbf{H}}{\partial t} dV = -\int_{V_i} \nabla \times \mathbf{N}_k \cdot \mathbf{E} dV - \int_{\partial V_i} \mathbf{N}_k \cdot \hat{n} \times \mathbf{E} dS. \tag{8}$$

By adopting upwind numerical flux to (7) and (8), the tangential fields on ∂V_i depend on the linear combination of the tangential fields on both sides of ∂V_i in two adjacent elements

$$\hat{n} \times \mathbf{H} = \hat{n} \times \mathbf{H}^i + \frac{Z^j}{Z^i + Z^j} \hat{n} \times \left(\mathbf{H}^j - \mathbf{H}^i\right) + \frac{1}{Z^i + Z^j} \hat{n} \times \left(\hat{n} \times \left(\mathbf{E}^i - \mathbf{E}^j\right)\right) - \frac{Z^j \mathbf{J}_{\mathrm{CKT}}}{Z^i + Z^j} \tag{9}$$

$$\hat{n} \times \mathbf{E} = \hat{n} \times \mathbf{E}^i + \frac{Y^j}{Y^i + Y^j} \hat{n} \times \left(\mathbf{E}^j - \mathbf{E}^i\right) + \frac{1}{Y^i + Y^j} \hat{n} \times \left(\hat{n} \times \left(\mathbf{H}^j - \mathbf{H}^i\right)\right) - \frac{\hat{n} \times \mathbf{J}_{\mathrm{CKT}}}{Y^i + Y^j}. \tag{10}$$

The superscript i or j represents the quantity corresponding to the ith element or adjacent jth element. $Z^i = 1/Y^i = (\mu^i/\varepsilon^i)^{1/2}$, $Z^j = 1/Y^j = (\mu^j/\varepsilon^j)^{1/2}$. $\mathbf{J}_{\mathrm{CKT}}$ equal to zero at the surfaces without lumped ports.

Substitute (9) and (10) into (7) and (8), and expand the electromagnetic fields with the second-order hierarchical vector basis functions, we can obtain the semi-discrete DG matrix equations

$$\varepsilon \mathbf{M}^i \frac{\partial \mathbf{e}^i}{\partial t} = \mathbf{S}^i \mathbf{h}^i + \mathbf{F}_{ee}^{ii} \mathbf{e}^i - \mathbf{F}_{ee}^{ij} \mathbf{e}^j - \mathbf{F}_{eh}^{ii} \mathbf{h}^i + \mathbf{F}_{eh}^{ij} h^j - \mathbf{C}^i \mathbf{e}^i - \mathbf{J}_e^i \tag{11}$$

$$\mu \mathbf{M}^i \frac{\partial \mathbf{h}^i}{\partial t} = -\mathbf{S}^i \mathbf{e}^i + \mathbf{F}_{hh}^{ii} \mathbf{h}^i - \mathbf{F}_{hh}^{ij} \mathbf{h}^j + \mathbf{F}_{he}^{ii} \mathbf{e}^i - \mathbf{F}_{he}^{ij} \mathbf{e}^j + \mathbf{J}_h^i. \tag{12}$$

The detailed expressions of all the matrix elements in (11) and (12) are summarized in the Appendix.

The leapfrog temporal integration scheme is used to generate the fully discrete DG matrix equations

$$\varepsilon \mathbf{M}^i \mathbf{e}_{n+1}^i + \frac{\Delta t}{2} \mathbf{C}^i \mathbf{e}_{n+1}^i + \frac{\Delta t}{2} \mathbf{J}_{e,n+1}^i = \varepsilon \mathbf{M}^i \mathbf{e}_n^i + \Delta \mathrm{t} \left[\mathbf{S}^i \mathbf{h}_{n+1/2}^i - \frac{\mathbf{J}_{e,n}^i}{2} + \mathbf{F}_{ee}^{ii} \mathbf{e}_n^i - \mathbf{F}_{ee}^{ij} \mathbf{e}_n^j - \mathbf{F}_{eh}^{ii} \mathbf{h}_{n+1/2}^i + \mathbf{F}_{eh}^{ij} \mathbf{h}_{n+1/2}^j - \frac{1}{2} \mathbf{C}^i \mathbf{e}_n^i \right] \tag{13}$$

$$\mu \mathbf{M}^i \mathbf{h}_{n+3/2}^i = \mu \mathbf{M}^i \mathbf{h}_{n+1/2}^i + \Delta \mathrm{t} \left[-\mathbf{S}^i \mathbf{e}_{n+1}^i + \mathbf{J}_{h,n+1}^i + \mathbf{F}_{hh}^{ii} \mathbf{h}_{n+1/2}^i - \mathbf{F}_{hh}^{ij} \mathbf{h}_{n+1/2}^j + \mathbf{F}_{he}^{ii} \mathbf{e}_{n+1}^i - \mathbf{F}_{he}^{ij} \mathbf{e}_{n+1}^j \right]. \tag{14}$$

The modified nodal analysis method is adopted to obtain the matrix equations for the lumped circuits [24]. The resultant circuit equations can be expressed as a functional relationship between the port currents $\mathbf{I}_n$ and port voltages $\mathbf{V}_n$

$$\mathbf{I}_n = f(\mathbf{V}_n). \tag{15}$$

The coupling relationship between the electromagnetic equation and circuit equation is constructed using the port voltage, port current, and the electric field of the port element

$$\mathbf{V}_n = -\int \mathbf{E}^i \cdot \hat{L} dL = -\sum_{k=1}^{N_e} e_{k,n}^i \int \mathbf{N}_k^i \cdot \hat{L} dL \tag{16}$$

$$\mathbf{J}_{\mathrm{CKT}} = \mathbf{I}_n / W \tag{17}$$

where $\hat{L}$ represents the unit vector from the ground to the potential point at the lumped port. W refers to the width of the lumped port.

The electromagnetic equations in (13) and (14) and the circuit equation in (15) can be combined into a whole synchronously solved marching-on-in-time system equation through (16) and (17). After solving this equation, we can obtain the port currents, the port voltages at the lumped ports, and the electromagnetic fields in the computational domain V.

B. Thermal Simulation

The thermal simulation is based on the transient heat conduction equation

$$\rho C_\rho \frac{\partial T}{\partial t} = \nabla \cdot (\kappa \nabla T) + Q \tag{18}$$

where T refers to the transient temperature distribution of the object, which is the unknown of this equation. ρ denotes the mass density. C_ρ is the specific heat capacity. κ represents the thermal conductivity. Q is the heat source, which means the thermal energy generated per unit time and unit volume.

Consider the commonly used convection boundary condition which describes the thermal transfer between the object surface and its surrounding environment

$$-\hat{n} \cdot \kappa \nabla T = h(T - T_{\mathrm{sur}}) \tag{19}$$

where T_{sur} represents the surrounding temperature. h refers to the convective heat transfer coefficient.

A standard process of the FETD method is used to solve the heat conduction equation. The tetrahedral mesh used for EM simulation is also adopted for thermal simulation. The unknown T in (18) is expanded by the second-order scalar interpolation basis functions [25]

$$N_k = (2L_k - 1)L_k \quad (k = 1, 2, 3, 4) \tag{20}$$

$$N_k = 4L_{k1}L_{k2} \quad (k = 5, 6, \ldots, 10) \tag{21}$$

where L_k is the volume coordinate related to node k of a tetrahedral element. L_{k1} and L_{k2} denote the volume coordinate related to the two nodes of one of the six edges, respectively.

Using the Galerkin testing method and Crank–Nicolson (CN) scheme for temporal discretization [31], we can obtain the final matrix equation for thermal simulation

$$\left([\mathbf{C}] + [\mathbf{K}]\frac{\Delta t}{2}\right)\{\tau_i\} = \left([\mathbf{C}] - [\mathbf{K}]\frac{\Delta t}{2}\right)\{\tau_{i-1}\} + \{\mathbf{f}\}\Delta t \tag{22}$$

where

$$[\mathbf{C}]_{kl} = \rho C_\rho \int_V N_k N_l dV \tag{23}$$

$$[\mathbf{K}]_{kl} = \kappa \int_V \nabla N_k \cdot \nabla N_l dV + h \int_S N_k N_l dS \tag{24}$$

$$\{\mathbf{f}\}_k = \int_V N_k Q dV + h \int_S N_k T_{\text{sur}} dS. \tag{25}$$

After solving (22), we can obtain the transient temperature distribution of the object.

C. Electromagnetic-Circuital-Thermal Coupling Mechanism

After electromagnetic–circuital co-simulation at each time step, we can obtain the corresponding electric field distribution $\mathbf{E}$. Then we can calculate the dissipated power at that time step

$$P = \sigma |\mathbf{E}|^2. \tag{26}$$

This dissipated power serves as the heat source Q in thermal simulation. According to the thermal simulation result at each time step, we can check if the temperature distribution changes. The changed temperature may influence temperature-dependent medium parameters such as permittivity, permeability, and conductivity. Thus, it will influence the electromagnetic–circuital co-simulation in the next time step. This process iterates until the current time step equals to the predetermined total number of time steps N_t.

In this article, we only consider the influence of temperature on conductivity. Their relationships are supposed to be

$$\sigma = \frac{\sigma_0}{1 + \alpha(T - T_i)} \tag{27}$$

where σ_0 is the conductivity at initial temperature T_i. α is the temperature coefficient of the material.

The strategy of temporal discretization for electromagnetic-circuital–thermal co-simulation also needs to be well-designed. In our work, the CN scheme is adopted for temporal discretization of thermal simulation, which is unconditionally stable. Leapfrog scheme is used for temporal discretization of electromagnetic–circuital co-simulation, which is explicit and conditionally stable. So Courant limit needs to be taken into account for electromagnetic–circuital co-simulation. The time step size of the ith element of the DGTD method Δt_i should satisfy [26]–[28]

$$c_i \Delta t_i \left[\frac{4\sqrt{5}}{3} + \frac{8}{3}\max\left(\sqrt{\frac{\mu_i}{\mu_j}}, \sqrt{\frac{\varepsilon_i}{\varepsilon_j}}\right)\right] < \frac{4V_i}{P_i} \tag{28}$$

where $c_i = 1/(\varepsilon_i \mu_i)^{1/2}$ is the speed of light. V_i refers to the volume of the ith element. P_i is the total area of four facets of the ith element. The subscript j represents one of the neighboring elements of the ith element. The time step size of all the elements is the same in this article, which is $\Delta t = \min\{\Delta t_i, i = 1, 2, \ldots, N\}$.

Since the temperature changes much slower than the electromagnetic fields, we can also adopt larger time step size for thermal simulation than for electromagnetic–circuital co-simulation to implement asynchronous electromagnetic–circuital–thermal co-simulation to accelerate the simulation process. The time step size of thermal simulation is chosen to be $k_{T-\text{EM}}$ times of the time step size of EM simulation

$$\Delta t_{\text{th}} = k_{T-\text{EM}} \Delta t_{\text{EM}} \tag{29}$$

where $k_{T-\text{EM}}$ is recommended to be smaller than 2000 to guarantee accuracy according to the numerical experiments in Section III. In the asynchronous electromagnetic-circuital–thermal co-simulation, the dissipated powers obtained by electromagnetic–circuital co-simulation of every $k_{T-\text{EM}}$ time steps are averaged as the heat source of thermal simulation.

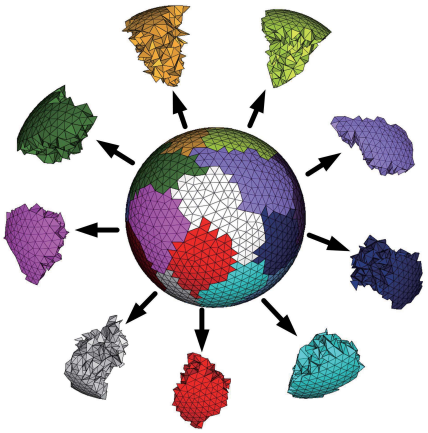

Fig. 2. Schematic of dividing the original meshes into different groups.

D. Parallel Strategies

Since the electromagnetic–circuital co-simulation and thermal simulation are weakly coupled, they are separately parallelized using message passing interface (MPI) technique to accelerate the electromagnetic-circuital–thermal co-simulation. There are mainly three stages for parallelization of both the electromagnetic–circuital co-simulation and thermal simulation, namely, mesh grouping, matrix filling and equation solving.

In the stage of mesh grouping, the original meshes are divided into different groups as shown in Fig. 2. Thus, each

process can handle one group of meshes. There are two important rules for good grouping: 1) the number of meshes for each group should be almost the same to guarantee load balance and 2) the interfaces between the meshes of different groups should be minimum to reduce inter-process communication. Thanks to the METIS software [29], we can easily group the original meshes satisfying the above two rules.

For electromagnetic–circuital co-simulation, each process computes the element matrices related to its own group of meshes during matrix filling stage. What calls for special attention is that the information of adjacent elements is needed when computing $\mathbf{F}_{ee}^{ij}$, $\mathbf{F}_{eh}^{ij}$, $\mathbf{F}_{he}^{ij}$, and $\mathbf{F}_{hh}^{ij}$ because inter-process communication is needed for the elements at the interfaces belonging to two adjacent groups. All the other matrices can be calculated directly by each process without inter-process communication. Similarly, in the stage of solving matrix equation, each process will solve many small element matrix equations related to its own meshes. However, inter-process communication is required when computing the matrix vector multiplication $\mathbf{F}_{ee}^{ij}\mathbf{e}^j$, $\mathbf{F}_{eh}^{ij}\mathbf{h}^j$, $\mathbf{F}_{he}^{ij}\mathbf{e}^j$, and $\mathbf{F}_{hh}^{ij}\mathbf{h}^j$ in (13) and (14) for the elements at the interfaces belonging to two adjacent groups. Since the elements at the interfaces account for a very small percentage of all the elements, the amount of inter-process communication of the DGTD method is quite small, resulting in a rather high parallel efficiency.

For thermal simulation, after the element matrices with their expressions in (23), (24), and (25) are computed in each process, the large global sparse matrix at the left-hand side of (22) need to be assembled using all the element matrices. The right-hand side of (22) can be calculated by each process in parallel. Finally, the final large matrix equation is solved using a parallel sparse direct solver named multifrontal massively parallel sparse direct solver (MUMPS) at each time step [30]. Since the FETD method needs to solve global sparse matrix equations, the parallel efficiency is relatively lower than the DGTD method due to the great amount of inter-process communication.

The standard definition of parallel efficiency is

$$\eta = \frac{T_s}{NT_N} \tag{30}$$

where T_s is the total CPU time when a problem is solved by a single process, while T_N is the total CPU time when the same problem is solved by N processes. In practice, if the problem to be solved cannot fit into a single process, we take the time for the smallest number of processes as the reference. The parallel efficiency is re-defined as

$$\eta = \frac{T_{N_r} N_r}{T_N N} \tag{31}$$

where T_{N_r} is the total CPU time taken by N_r processes, and T_N is the total CPU time taken by N processes. In this case, the smallest number of processes is N_r.

III. Numerical Results

In this section, four numerical examples are given to validate the electromagnetic–circuital co-simulation method, thermal simulation method, and the electromagnetic–circuital-thermal co-simulation method. The computational platform adopted for the testing of parallel efficiency is a High Performance Cluster of Beijing Super Cloud Computing Center (BSCC). There are 100 compute nodes in the cluster. Each node is equipped with AMD EPYC 7452 CPU with 32 cores and 256-GB RAM. Each core supports two processes. Other numerical results are obtained on a workstation with Intel Xeon E5-1660 CPU with eight cores and 128-GB RAM.

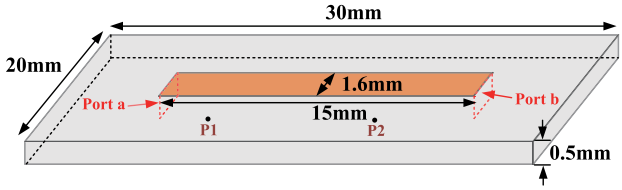

Fig. 3. Model of a microstrip line structure.

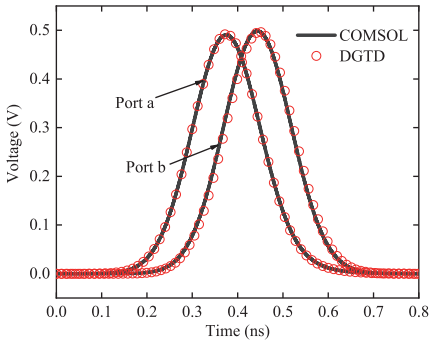

Fig. 4. Voltage waveforms at port a and port b.

A. Validation of Electromagnetic–Circuital Co-Simulation Method by a Microstrip Line Structure

As shown in Fig. 3, a microstrip line resides 0.5 mm above the ground plane. The length and the width of microstrip line are 15 and 1.6 mm, respectively. The length and width of the ground plane are 30 and 20 mm, respectively. The relative dielectric constant of the substrate is 2.0. Two lumped ports are defined at port a and port b, respectively. Port a is driven by a Gaussian pulse source in series with a 50-Ω resistor. Port b is connected with a 50-Ω resistor.

First, the model is discretized into 3523 tetrahedron elements. The total simulation time is set to be 0.8 ns. The total number of time steps is 30 000. Second-order hierarchical vector basis function is adopted. The voltages at port a and port b are obtained by the DGTD method as shown in Fig. 4. Besides, the transient electric field components at two randomly chosen sampling points P1 (−6.5, 0, 0.25 mm) and P2 (2.5, 0, 0.25 mm) are calculated as shown in Fig. 5. The transient electric field distribution on the plane of $z = 0.25$ mm at 0.25 ns is given in Fig. 6. All the results obtained by our proposed method agree well with those of COMSOL software. Besides, the CPU times and the memory requirements of the proposed method and the COMSOL software are compared in Table I for all the numerical examples in this section. Both the proposed method and the COMSOL software use parallel

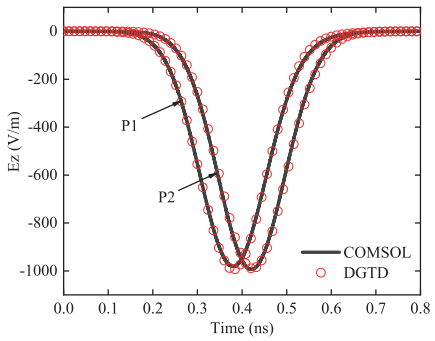

Fig. 5. Transient electric field components at two randomly chosen sampling points P1 and P2.

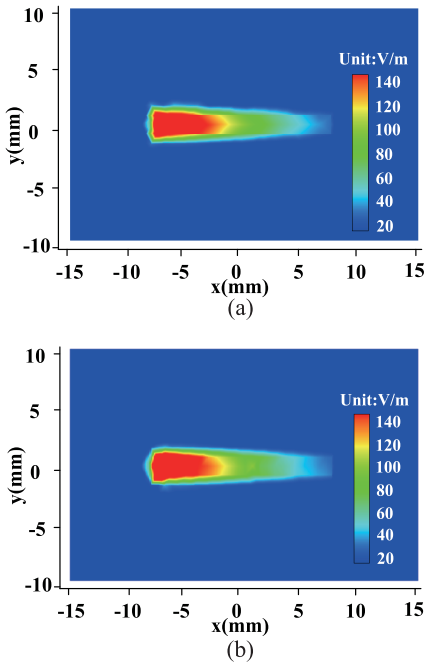

Fig. 6. The transient electric field distribution on the plane of $z = 0.25$ mm at 0.25 ns obtained by (a) COMSOL software and (b) proposed method.

computing with eight cores. Obviously, the CPU time and memory consumption of the proposed method are less than the COMSOL software.

Second, both the first-order vector basis functions and second-order vector basis functions are used, respectively, to compare their performance. The voltage value at port a is recorded. The average relative error is calculated using (32). As shown in Table II, when the accuracy of two kinds of basis functions is similar, the number of elements, memory requirement, and CPU time needed when using second-order basis functions are much less than those when using first-order basis functions

$$\text{Error} = \frac{1}{N_t}\sum_{n=1}^{N_t}\frac{\left|\mathrm{V}^n_{\mathrm{DGTD}} - \mathrm{V}^n_{\mathrm{COMSOL}}\right|}{\left|\mathrm{V}^n_{\mathrm{COMSOL}}\right|} \tag{32}$$

where N_t is the total number of time steps, and $\mathrm{V}^n_{\mathrm{DGTD}}$ and $\mathrm{V}^n_{\mathrm{COMSOL}}$ are the voltage values at time step n calculated by the DGTD method and COMSOL software, respectively.

TABLE I

CPU TIME AND THE MEMORY REQUIREMENT OF THE PROPOSED METHOD AND THE COMSOL SOFTWARE FOR THE FOUR NUMERICAL EXAMPLES

	Method	Number of Elements	CPU Times	Memory Requirements
A	Proposed	3523	184 s	329 MB
	COMSOL	3509	791 s	1677 MB
B	Proposed	49396	71 s	837 MB
	COMSOL	49396	190 s	2594 MB
C	Proposed	3523	2955 s	496 MB
	COMSOL	3509	7387 s	1537 MB
D	Proposed (EM-Circuit)	16385	2.5 h	1388 MB
	COMSOL (EM-Circuit)	16254	5.3 h	4302 MB
	Proposed (EM-Circuit-Thermal)	16385	2.7 h	1568 MB
	COMSOL (EM-Circuit-Thermal)	16254	5.8 h	4390 MB

TABLE II

PERFORMANCE OF DIFFERENT ORDER BASIS FUNCTIONS

	First Order	Second Order
Mesh Size (mm)	0.8	2
Number of Elements	41695	3523
Memory Requirement (MB)	384	329
CPU Time (s)	1207	184
Average Relative Error (%)	0.43	0.39

TABLE III

CPU TIME AND PARALLEL EFFICIENCY OF THE DGTD METHOD

Number of Processes	CPU Time (h)	Parallel Efficiency
64	9.6	100% (Baseline)
128	4.9	98.3%
192	3.4	94.6%
256	2.6	91%
512	1.9	85.7%

Third, the parallel performance of the proposed method is assessed. The model is discretized into 158 380 elements. Second-order hierarchical vector basis function is adopted. The CPU time corresponding to 64, 128, 192, 256, and 512 processes is recorded. Then the parallel efficiency of the proposed method is computed as given in Table III. It can be observed that the DGTD method has a quite good parallel performance.

B. Validation of Thermal Simulation Method by Dual-Polarized Dipole Antenna Structure

The thermal simulation of a 3 × 3 base station antenna array is carried out as the second example. As shown in Fig. 7, the structure consists of nine dual-polarized dipole antennas, a ground plane, and six heat source blocks. The sizes of the antenna element and the ground plane are 33.125 × 33.125 × 25 mm^3 and 214 × 185 × 1.875 mm^3, respectively. The detailed dimensions of the geometry are summarized in Table IV. The material of the whole structure is aluminum. The total power of the six heat source blocks is 19.2 W, which is used to imitate the heating of RF circuits. All boundary surfaces of the structure are supposed to be the

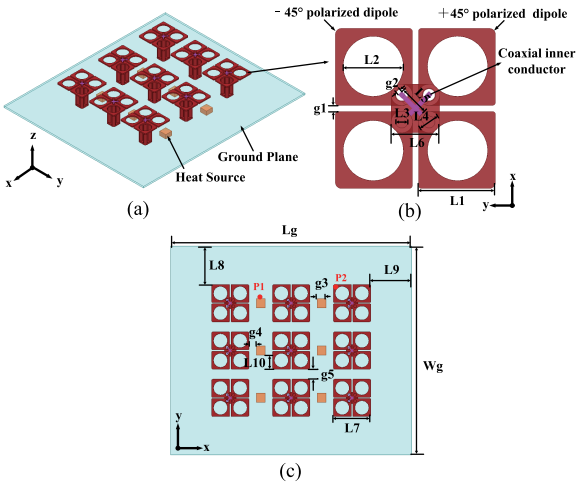

Fig. 7. Base station antenna array. (a) 3-D view. (b) Antenna element. (c) Top view.

TABLE IV
DETAILED DIMENSIONS OF THE GEOMETRY (UNIT: mm)

L1	L2	L3	L4	L5	L6
15.3	11.5	2.5	3.75	4.4	8.7
L7	**L8**	**L9**	**L10**	**Lg**	**Wg**
33.125	48.6	43.6	11	214	185
g1	**g2**	**g3**	**g4**	**g5**	
1.25	1	8	6.2	8.875	

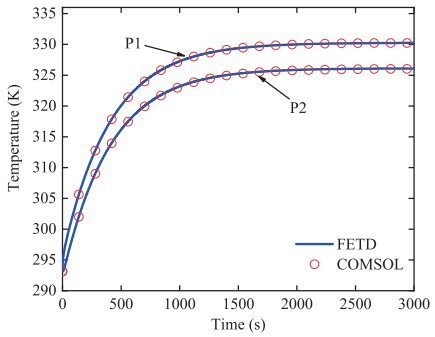

Fig. 8. Temperatures at two randomly chosen sampling points P1 and P2.

convective boundary conditions with heat transfer coefficient $h = 5\ \mathrm{W/(m^2 \cdot K)}$. The ambient temperature and initial temperature of the structure are 293.15 K. The structure is discretized into 49 396 tetrahedron elements. The total simulation time is 3000 s. The total number of time steps is 3000. Second-order scalar basis function is adopted. The temperatures at two randomly chosen sampling points P1 (92, 100, 0 mm) and P2 (31, 88, −26 mm) are calculated as shown in Fig. 8. In addition, the 3-D temperature distributions of the structure obtained by the proposed method and COMSOL software at 190 s are also demonstrated in Fig. 9. Good agreement can be observed. The CPU times and memory requirements of the proposed method and the COMSOL software are given in Table I.

Both the first-order scalar basis functions and second-order scalar basis functions are adopted, respectively, to compare

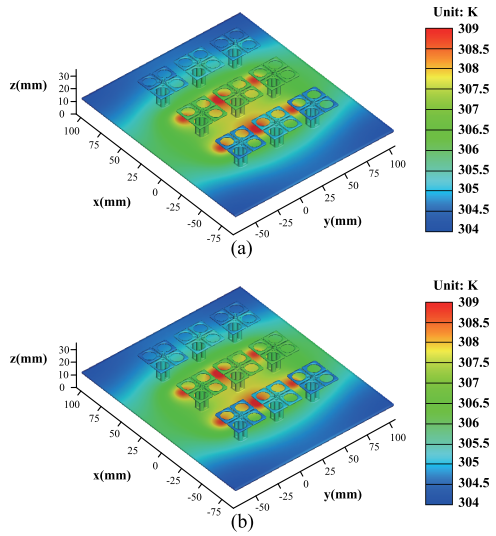

Fig. 9. 3-D temperature distributions of the structure at 190 s obtained by (a) COMSOL software and (b) proposed method.

TABLE V
PERFORMANCE OF DIFFERENT ORDER BASIS FUNCTIONS

	First Order	Second Order
Mesh Size (mm)	0.6	1.6
Number of Elements	518068	49396
Memory Requirement (MB)	979	837
CPU Time (s)	129	71
Average Relative Error (%)	0.01	0.01

TABLE VI
CPU TIME AND PARALLEL EFFICIENCY OF THE FETD METHOD

Number of Processes	CPU Time (h)	Parallel Efficiency
8	2.7	100% (Baseline)
16	1.6	85%
32	1	67.5%
56	0.96	40%
64	0.92	36%

their performance. The temperatures of six randomly chosen observation points are recorded. The average relative error is calculated by (33). As shown in Table V, when the accuracy of two kinds of basis functions is the same, the number of elements, memory requirement, and CPU time needed when using second-order basis functions are less than those when using first-order basis functions

$$\mathrm{Error} = \frac{1}{M}\sum_{p=1}^{M}\left(\frac{1}{N_t}\sum_{n=1}^{N_t}\frac{\left|\mathrm{T}_{\mathrm{FETD}}^{n,p} - \mathrm{T}_{\mathrm{COMSOL}}^{n,p}\right|}{\left|\mathrm{T}_{\mathrm{COMSOL}}^{n,p}\right|}\right) \tag{33}$$

where N_t is the total number of time steps, M is the total number of observation points, and $\mathrm{T}_{\mathrm{FETD}}^{n,p}$ and $\mathrm{T}_{\mathrm{COMSOL}}^{n,p}$ are the temperatures of the pth observation point at time step n calculated using the FETD method and COMSOL software, respectively.

Finally, the parallel performance of the proposed method is assessed. The model is discretized into 333 087 elements. The CPU time corresponding to 8, 16, 32, 56, and 64 processes is recorded. Then the parallel efficiency of the proposed method is computed given in Table VI. The parallel efficiency of

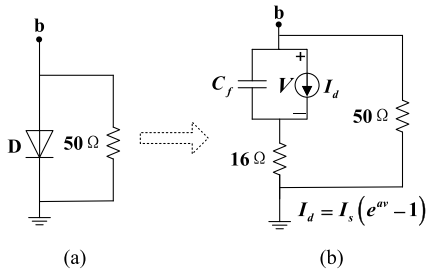

Fig. 10. (a) Circuit at port b. (b) Equivalent circuit model.

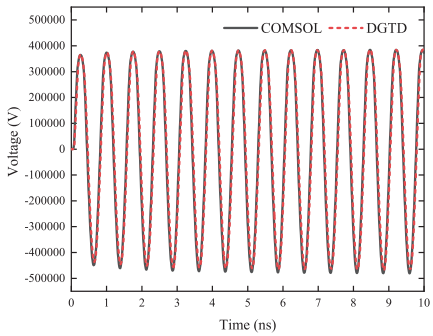

Fig. 11. Voltage waveforms at port b.

the FETD method decreases faster compared with the DGTD method.

C. Electromagnetic–Circuital–Thermal Co-Simulation of a Microstrip Line Loaded With a Diode

The dimension of the microstrip line structure is the same as the one in Fig. 3. Port a is driven by a sinusoidal voltage source in series with a 50-Ω resistor. Port b is connected with a diode in parallel with a 50-Ω resistor, the equivalent circuit model of which is shown in Fig. 10. The electromagnetic parameters of the substrate are $\varepsilon_r = 2.0$, $\sigma_0 = 0.1$. The thermal parameters are $\rho = 2330\ \text{kg/m}^3$, $C_\rho = 704\ \text{J/(kg} \cdot \text{K)}$, $\alpha = 0.01\ 1/\text{K}$, and $\kappa = 30\ \text{W/(m} \cdot \text{K)}$. In the thermal simulation, convective boundary condition is applied on all boundary surfaces with the heat transfer coefficient $h = 15\ \text{W/(m}^2 \cdot \text{K)}$. In addition, the ambient and initial temperatures are 293.15 K. The structure is discretized into 3523 tetrahedral elements. The total simulation time is set to be 10 ns. The total number of time steps is 250 000. The second-order vector basis function is used for electromagnetic simulation, while the first-order scalar basis function is adopted for thermal simulation.

First, the time step sizes for both electromagnetic–circuital and thermal simulations are chosen to be the same. The voltage at port b is shown in Fig. 11. Besides, the transient electric field component at a randomly chosen sampling point P (2.5, 0, 0.25 mm) is calculated as shown in Fig. 12. The temperature distribution on the plane of $z = 0.25$ mm at 0.5 ns is shown in Fig. 13. All the results obtained by our proposed method agree well with those of COMSOL software.

Second, asynchronous electromagnetic-circuital–thermal co-simulation is tested. The temperature curves at a randomly chosen sampling point P (−6.5 mm, 0 mm, 0.25 mm)

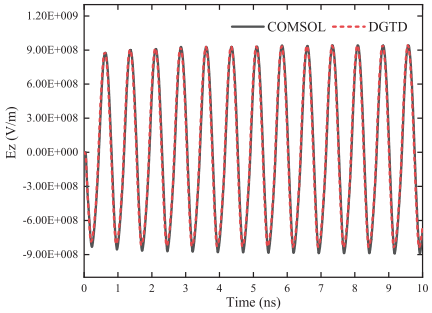

Fig. 12. Transient electric field component at a randomly chosen sampling point P (2.5, 0, 0.25 mm).

TABLE VII
CPU TIMES CORRESPONDING TO DIFFERENT THERMAL TIME STEP SIZES

k_{T-EM}	CPU Times of Thermal Simulation (s)	CPU Times of Total Time(s)
1	458	2955
2000	261	2751

TABLE VIII
CPU TIMES CORRESPONDING TO DIFFERENT THERMAL TIME STEP SIZES

k_{T-EM}	CPU Times of Thermal Simulation (s)	CPU Times of Total Time(s)
1	1197	9720
2000	700	9221

is computed using different thermal time steps $k_{T-\text{EM}} = 1, 1000, 2000, 5000, 8000$ as shown in Fig. 14. The transient electric field distributions on the plane of $z = 0.25$ mm at 4 ns with $k_{T-\text{EM}} = 1, 2000, 8000$ are displayed in Fig. 15. The results corresponding to $k_{T-\text{EM}} = 2000$ show small differences with the cases of $k_{T-\text{EM}} = 1$. So we recommend $k_{T-\text{EM}} = 2000$ to guarantee accuracy. Besides, the CPU time of $k_{T-\text{EM}} = 1$ and 2000 is given in Table VII. It can be observed that the CPU time of thermal simulation with $k_{T-\text{EM}} = 2000$ is reduced by over 43% compared with $k_{T-\text{EM}} = 1$.

D. Electromagnetic–Circuital–Thermal Co-Simulation of a MESFET Microwave Power Amplifier

A MESFET microwave power amplifier is analyzed as the last example. The microstrip matching network is shown in Fig. 16(a). The input port a and the output port b are driven by dc sources with amplitudes $V_{\text{GG}} = -0.81$ and $V_{\text{DD}} = 18.96$. An extra sinusoidal voltage source operating at 6 GHz is applied at port a. A MESFET is connected with ports G and D. The equivalent circuit models for the lumped circuits connected with the four ports are shown in Fig. 16(b). The microstrip matching network is discretized into 16 385 tetrahedron elements. The total simulation time is set to be 10 ns. The total number of time steps is 200 000. The second-order vector basis function is used for electromagnetic simulation, while the first-order scalar basis function is adopted for thermal simulation.

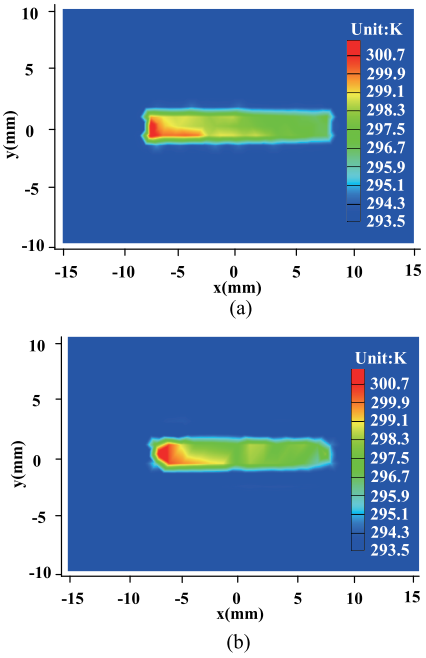

Fig. 13. Temperature distributions of the structure on the plane of $z = 0.25$ mm at 0.5 ns obtained by (a) COMSOL software and (b) proposed method.

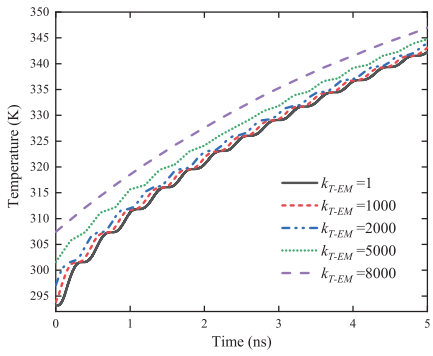

Fig. 14. Temperature curves corresponding to different thermal time step sizes.

First, the electromagnetic–circuital co-simulation and the electromagnetic–circuital–thermal co-simulation are carried out to further verify the accuracy of the proposed method. In the electromagnetic–circuital co-simulation, the substrate is supposed to be lossless with $\varepsilon_r = 2.33$. In the electromagnetic–circuital–thermal co-simulation, the relative dielectric constant of the substrate keeps unchanged. But the loss of the substrate is considered with $\sigma_0 = 0.1$. The thermal parameters are $\rho = 2330\ \mathrm{kg/m^3}$, $C_\rho = 1 \times 10^{-8}\ \mathrm{J/(kg \cdot K)}$, $\alpha = 0.1\ \mathrm{(1/K)}$, $\kappa = 9 \times 10^5\ \mathrm{W/(m \cdot K)}$. In the thermal simulation, all boundary surfaces of the structure are imposed convective boundary conditions with heat transfer coefficient $h = 0.1\ \mathrm{W/(m^2 \cdot K)}$. The ambient and initial temperatures are 293.15 K. An extra heat source of 36 kW is applied at the position of the MESFET to imitate its heating effect. The voltage waveforms at port G, port D, port a, and port b obtained from the proposed method agree well with those of COMSOL software in Fig. 17. Significant changes can be observed in

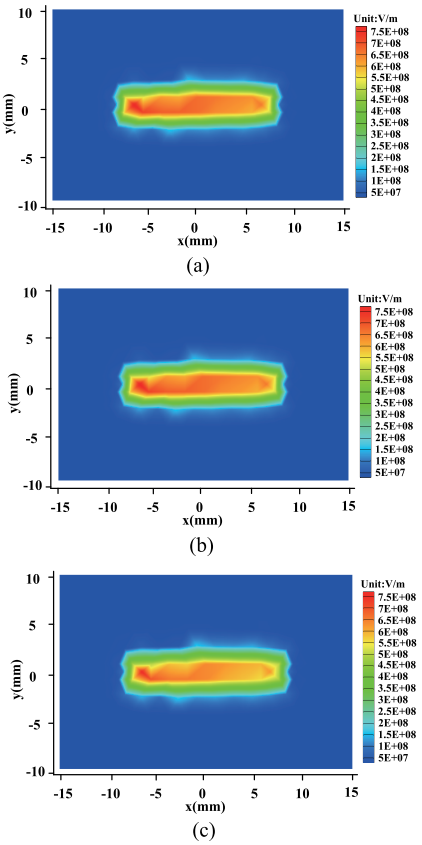

Fig. 15. Transient electric field distribution on the plane of $z = 0.25$ mm at 4 ns obtained with (a) $k_{T-\mathrm{EM}} = 1$, (b) $k_{T-\mathrm{EM}} = 2000$, and (c) $k_{T-\mathrm{EM}} = 8000$.

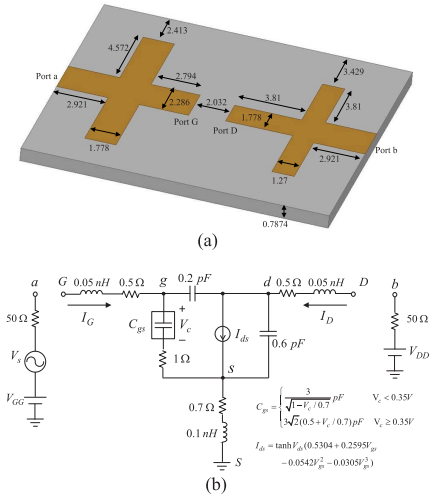

Fig. 16. Microwave power amplifier. (a) Microstrip matching network. (b) Equivalent circuit models of MESFET, source port termination, and loading port termination.

the voltage waveforms of Fig. 17(c) and (d) compared with those of Fig. 17(a) and (b), which means that the thermal effect can greatly influence the electrical property of the power amplifier. It cannot be ignored if a near-reality simulation result is expected. Moreover, the temperature distributions on the plane of $z = 0.7874$ mm at 9.5 ns obtained by the proposed

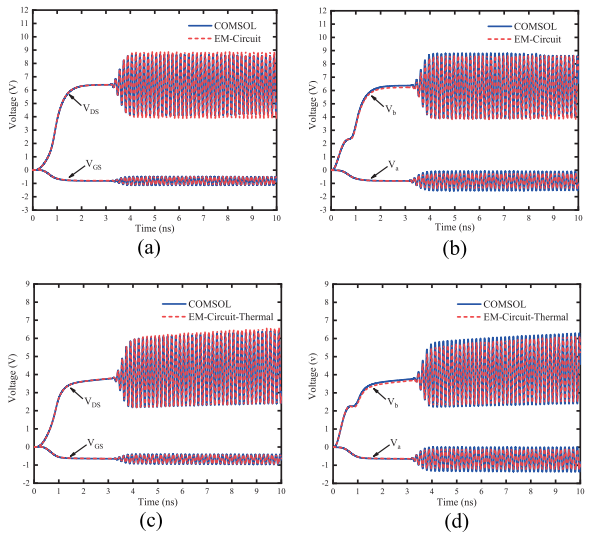

Fig. 17. (a) Voltages at port G and port D obtained by electromagnetic–circuital co-simulation. (b) Voltages at port a and port b obtained by electromagnetic–circuital co-simulation. (c) Voltages at port G and port D obtained by electromagnetic–circuital–thermal co-simulation. (d) Voltages at port a and port b obtained by electromagnetic–circuital–thermal co-simulation.

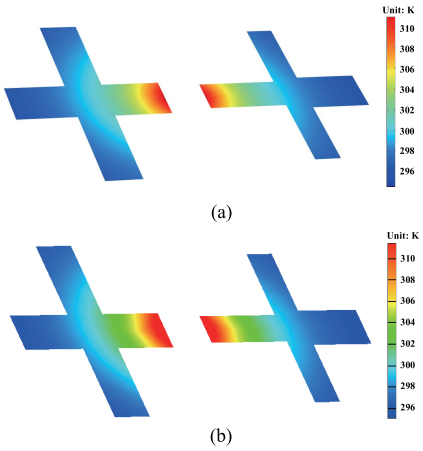

Fig. 18. Temperature distributions on the microstrip structures of the matching network at 9.5 ns obtained by (a) COMSOL software and (b) proposed method.

method and COMSOL software are shown in Fig. 18. A good agreement can be observed.

Second, we perform a small-signal analysis to calculate the *S*-parameters of the microwave amplifier. Once the system reaches its steady state, a modulated Gaussian pulse centered at 6 GHz is added on top of the dc signal, while the active device still operates in the linear region. Same process as above, the electromagnetic–circuital co-simulation and the electromagnetic–circuital–thermal co-simulation of the model are carried out. The electrical and thermal parameters remain unchanged. The voltage waveforms of port G, port D, port a, and port b are shown in Fig. 19. Then we use the voltages at Port a and Port b to calculate the *S*-parameters of the MESFET microwave amplifier. Fig. 20 shows the S11 and S21 curves based on electromagnetic–circuital co-simulation and electromagnetic-circuital–thermal co-simulation. Apparent

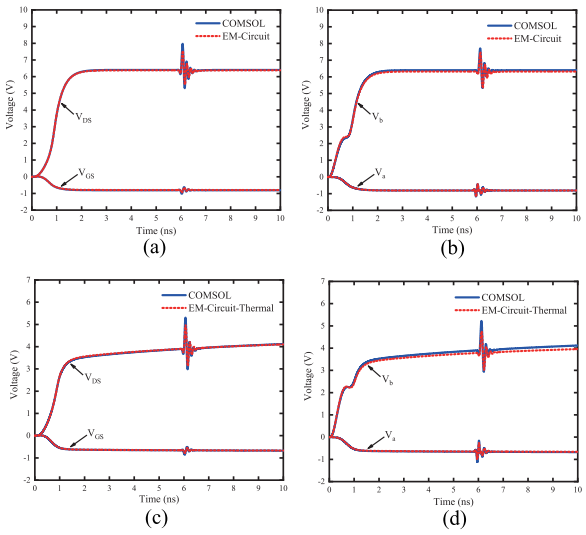

Fig. 19. (a) Voltages at port G and port D obtained by electromagnetic–circuital co-simulation. (b) Voltages at port a and port b obtained by electromagnetic–circuital co-simulation. (c) Voltages at port G and port D obtained by electromagnetic–circuital–thermal co-simulation. (d) Voltages at port a and port b obtained by electromagnetic–circuital–thermal co-simulation.

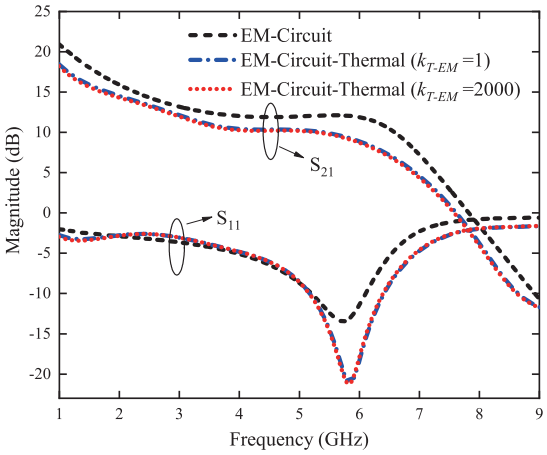

Fig. 20. S11 and S21 curves based on electromagnetic–circuital co-simulation, electromagnetic-circuital–thermal co-simulation with $k_{T-\mathrm{EM}} = 1$ and electromagnetic-circuital–thermal co-simulation with $k_{T-\mathrm{EM}} = 2000$.

differences induced by the thermal effect can be observed in Fig. 20, which proved the importance and necessity of electromagnetic–circuital-thermal co-simulation.

Finally, asynchronous electromagnetic–circuital–thermal co-simulation is tested with $k_{T-\mathrm{EM}} = 2000$ compared with the synchronous electromagnetic–circuital-thermal co-simulation with $k_{T-\mathrm{EM}} = 1$. The S11 and S21 curves are shown in Fig. 20. The results obtained by asynchronous co-simulation agree well with those obtained by synchronous co-simulation. Besides, the corresponding CPU times are given in Table VIII. More than 40% of the CPU time can be saved for thermal simulation with asynchronous electromagnetic–circuital–thermal co-simulation.

IV. Conclusion

An efficient transient electromagnetic–circuital–thermal co-simulation method is proposed in this article. The electromagnetic simulation, circuit simulation, and thermal

simulation are based on higher order DGTD method, modified nodal analysis method, and higher order FETD method, respectively. A physics-based coupling mechanism is constructed to achieve reasonable and accurate multiphysics simulation. Large-scale parallel technique is also implemented to further accelerate the whole simulation process. The proposed method provides a very effective and powerful solution scheme for electromagnetic–circuital–thermal co-simulation, which can be widely applied for the design of electronic components and systems with coupled electromagnetic, circuital, and thermal phenomena.

APPENDIX

$$\left[\mathbf{M}^i\right]_{kl} = \int_{V_i} \mathbf{N}_k^i \cdot \mathbf{N}_l^i dV \tag{34}$$

$$\left[\mathbf{S}^i\right]_{kl} = \int_{V_i} \mathbf{N}_k^i \cdot \left(\nabla \times \mathbf{N}_l^i\right) dV \tag{35}$$

$$\left[\mathbf{F}_{eh}^{ii}\right]_{kl} = \frac{Z^j}{Z^i + Z^j} \int_{\partial V_i} \mathbf{N}_k^i \cdot \left(\hat{n} \times \mathbf{N}_l^i\right) dS \tag{36}$$

$$\left[\mathbf{F}_{eh}^{ij}\right]_{kl} = \frac{Z^j}{Z^i + Z^j} \int_{\partial V_i} \mathbf{N}_k^i \cdot \left(\hat{n} \times \mathbf{N}_l^j\right) dS \tag{37}$$

$$\left[\mathbf{F}_{he}^{ii}\right]_{kl} = \frac{Y^j}{Y^i + Y^j} \int_{\partial V_i} \mathbf{N}_k^i \cdot \left(\hat{n} \times \mathbf{N}_l^i\right) dS \tag{38}$$

$$\left[\mathbf{F}_{he}^{ij}\right]_{kl} = \frac{Y^j}{Y^i + Y^j} \int_{\partial V_i} \mathbf{N}_k^i \cdot \left(\hat{n} \times \mathbf{N}_l^j\right) dS \tag{39}$$

$$\left[\mathbf{F}_{ee}^{ii}\right]_{kl} = \frac{1}{Z^i + Z^j} \int_{\partial V_i} \mathbf{N}_k^i \cdot \left(\hat{n} \times \hat{n} \times \mathbf{N}_l^i\right) dS \tag{40}$$

$$\left[\mathbf{F}_{ee}^{ij}\right]_{kl} = \frac{1}{Z^i + Z^j} \int_{\partial V_i} \mathbf{N}_k^i \cdot \left(\hat{n} \times \hat{n} \times \mathbf{N}_l^j\right) dS \tag{41}$$

$$\left[\mathbf{F}_{hh}^{ii}\right]_{kl} = \frac{1}{Y^i + Y^j} \int_{\partial V_i} \mathbf{N}_k^i \cdot \left(\hat{n} \times \hat{n} \times \mathbf{N}_l^i\right) dS \tag{42}$$

$$\left[\mathbf{F}_{hh}^{ij}\right]_{kl} = \frac{1}{Y^i + Y^j} \int_{\partial V_i} \mathbf{N}_k^i \cdot \left(\hat{n} \times \hat{n} \times \mathbf{N}_l^j\right) dS \tag{43}$$

$$\left[\mathbf{C}^i\right]_{kl} = \int_{V_i} \sigma \mathbf{N}_k^i \cdot \mathbf{N}_l^i dV \tag{44}$$

$$\left[\mathbf{J}_e^i\right]_k = \frac{Z^j}{Z^i + Z^j} \int_{\partial V_i} \mathbf{N}_k^i \cdot \mathbf{J}_{\mathrm{CKT}} dS \tag{45}$$

$$\left[\mathbf{J}_h^i\right]_k = \frac{1}{Y^i + Y^j} \int_{\partial V_i} \mathbf{N}_k^i \cdot \hat{n} \times \mathbf{J}_{\mathrm{CKT}} dS. \tag{46}$$

REFERENCES

[1] K. Niu, Z. Huang, X. Ren, M. Li, B. Wu, and X. Wu, "An optimized 3-D HIE-FDTD method with reduced numerical dispersion," *IEEE Trans. Antennas Propag.*, vol. 66, no. 11, pp. 6435–6440, Nov. 2018.

[2] K.-P. Ma, M. Chen, B. Houshmand, Y. Qian, and T. Itoh, "Global time-domain full-wave analysis of microwave circuits involving highly nonlinear phenomena and EMC effects," *IEEE Trans. Microw. Theory Techn.*, vol. 47, no. 6, pp. 859–866, Jun. 1999.

[3] S. Grivet-Talocia, I. S. Stievano, and F. G. Canavero, "Hybridization of FDTD and device behavioral-modeling techniques [interconnected digital I/O ports]," *IEEE Trans. Electromagn. Compat.*, vol. 45, no. 1, pp. 31–42, Apr. 2003.

[4] R.-S. Chen, L. Du, Z. Ye, and Y. Yang, "An efficient algorithm for implementing the Crank–Nicolson scheme in the mixed finite-element time-domain method," *IEEE Trans. Antennas Propag.*, vol. 57, no. 10, pp. 3216–3222, Oct. 2009.

[5] H.-P. Tsai, Y. Wang, and T. Itoh, "An unconditionally stable extended (USE) finite-element time-domain solution of active nonlinear microwave circuits using perfectly matched layers," *IEEE Trans. Microw. Theory Techn.*, vol. 50, no. 10, pp. 2226–2232, Oct. 2002.

[6] R. Wang and J.-M. Jin, "Incorporation of multiport lumped networks into the hybrid time-domain finite-element analysis," *IEEE Trans. Microw. Theory Techn.*, vol. 57, no. 8, pp. 2030–2037, Aug. 2009.

[7] K. Aygün, B. C. Fischer, J. Meng, B. Shanker, and E. Michielssen, "A fast hybrid field-circuit simulator for transient analysis of microwave circuits," *IEEE Trans. Microw. Theory Techn.*, vol. 52, no. 2, pp. 573–583, Feb. 2004.

[8] H. H. Zhang, L. J. Jiang, and H. M. Yao, "Embedding the behavior macromodel into TDIE for transient field-circuit simulations," *IEEE Trans. Antennas Propag.*, vol. 64, no. 7, pp. 3233–3238, Jul. 2016.

[9] P. Li, L. J. Jiang, and H. Bagci, "Cosimulation of electromagnetics-circuit systems exploiting DGTD and MNA," *IEEE Trans. Compon., Packag., Manuf. Technol.*, vol. 4, no. 6, pp. 1052–1061, Jun. 2014.

[10] H. H. Zhang, L. J. Jiang, H. M. Yao, and Y. Zhang, "Transient heterogeneous electromagnetic simulation with DGTD and behavioral macromodel," *IEEE Trans. Electromagn. Compat.*, vol. 59, no. 4, pp. 1152–1160, Aug. 2017.

[11] L. Ma *et al.*, "Experimental validation of a combined electromagnetic and thermal FDTD model of a microwave heating process," *IEEE Trans. Microw. Theory Techn.*, vol. 43, no. 11, pp. 2565–2572, Nov. 1995.

[12] F. Torres and B. Jecko, "Complete FDTD analysis of microwave heating processes in frequency-dependent and temperature-dependent media," *IEEE Trans. Microw. Theory Techn.*, vol. 45, no. 1, pp. 108–117, Jan. 1997.

[13] T. Lu and J.-M. Jin, "Electrical-thermal co-simulation for analysis of high-power RF/microwave components," *IEEE Trans. Electromagn. Compat.*, vol. 59, no. 1, pp. 93–102, Feb. 2017.

[14] H. H. Zhang *et al.*, "Electromagnetic-thermal analysis of human head exposed to cell phones with the consideration of radiative cooling," *IEEE Antennas Wireless Propag. Lett.*, vol. 17, no. 9, pp. 1584–1587, Sep. 2018.

[15] Y. Dong, M. Tang, P. Li, and J. Mao, "Transient electromagnetic-thermal simulation of dispersive media using DGTD method," *IEEE Trans. Electromagn. Compat.*, vol. 61, no. 4, pp. 1305–1313, Aug. 2019.

[16] Y. Xue, Q. Ren, J. Chen, and Y. Zhou, "Transient electromagnetic–thermal cosimulation for micrometer-level components," *IEEE Trans. Microw. Theory Techn.*, vol. 69, no. 10, pp. 4341–4351, Oct. 2021.

[17] H. H. Zhang *et al.*, "Electromagnetic-circuital-thermal multiphysics simulation method: A review," *Prog. Electromagn. Res.*, vol. 169, pp. 87–101, 2020.

[18] S. Wunsche, C. Clauss, P. Schwarz, and F. Winkler, "Electro-thermal circuit simulation using simulator coupling," *IEEE Trans. Very Large Scale Integr. (VLSI) Syst.*, vol. 5, no. 3, pp. 277–282, Sep. 1997.

[19] H. M. Gutierrez, C. E. Christoffersen, and M. B. Steer, "An integrated environment for the simulation of electrical, thermal and electromagnetic interactions in high-performance integrated circuits," in *Proc. IEEE 8th Topical Meeting Electr. Perform. Electron. Packag.*, Oct. 1999, pp. 217–220.

[20] A. Morandi, M. Fabbri, and P. L. Ribani, "Coupled electromagnetic-thermal model and equivalent circuit of a magnetic shield type SFCL," *IEEE Trans. Appl. Supercond.*, vol. 23, no. 3, Jun. 2013, Art. no. 5602705.

[21] K. Fukahori and P. R. Gray, "Computer simulation of integrated circuits in the presence of electrothermal interaction," *IEEE J. Solid-State Circuits*, vol. JSSC-11, no. 6, pp. 834–846, Dec. 1976.

[22] J. P. Webb, "Hierarchal vector basis functions of arbitrary order for triangular and tetrahedral finite elements," *IEEE Trans. Antennas Propag.*, vol. 47, no. 8, pp. 1244–1253, Aug. 1999.

[23] L. S. Andersen and J. L. Volakis, "Hierarchical tangential vector finite elements for tetrahedra," *IEEE Microw. Guided Wave Lett.*, vol. 8, no. 3, pp. 127–129, Mar. 1998.

[24] C.-W. Ho, A. E. Ruehli, and P. A. Brennan, "The modified nodal approach to network analysis," *IEEE Trans. Circuits Syst.*, vol. CAS-22, no. 6, pp. 504–509, Jun. 1975.

[25] J. M. Jin, *The Finite Element Method in Electromagnetics*. Hoboken, NJ, USA: Wiley, 2015.

[26] L. Fezoui, S. Lanteri, S. Lohrengel, and S. Piperno, "Convergence and stability of a discontinuous Galerkin time-domain method for the 3D heterogeneous Maxwell equations on unstructured meshes," *ESAIM, Math. Model. Numer. Anal.*, vol. 39, no. 6, pp. 1149–1176, 2005.

[27] S. Dosopoulos and J.-F. Lee, "Interconnect and lumped elements modeling in interior penalty discontinuous Galerkin time-domain methods," *J. Comput. Phys.*, vol. 229, no. 22, pp. 8521–8536, Aug. 2010.
[28] P. Li and L. J. Jiang, "Integration of arbitrary lumped multiport circuit networks into the discontinuous Galerkin time-domain analysis," *IEEE Trans. Microw. Theory Techn.*, vol. 61, no. 7, pp. 2525–2534, Jul. 2013.
[29] T. Pospišek and D. Konečny, "METIS," in *Data and Mobility*. Berlin, Germany: Springer, 2010.
[30] P. Amestoy, I. S. Duff, J. Koster, and J.-Y. l'Excellent, "Multifrontal massively parallel solver (MUMPS version 4.3) users' guide," LIP, CERFACS, Toulouse, France, Tech. Rep., 2003.
[31] E. L. Tan, "Efficient algorithms for Crank–Nicolson-based finite-difference time-domain methods," *IEEE Trans. Microw. Theory Techn.*, vol. 56, no. 2, pp. 408–413, Feb. 2008.

Huan Huan Zhang (Member, IEEE) received the Ph.D. degree in electromagnetic (EM) fields and microwave technology from the Nanjing University of Science and Technology, Nanjing, China, in 2015.

He was a Post-Doctoral Research Fellow with the Center of Electromagnetics and Optics, The University of Hong Kong, Hong Kong, from 2015 to 2016. He is currently an Associate Professor with the School of Electronic Engineering, Xidian University, Xi'an, China. His current research interests include multiphysics simulation, antenna theory, bioelectromagnetics, and computational electromagnetics.

Dr. Zhang was a recipient of the 2019 Young Scientist Award of the International Applied Computational Electromagnetics Society Symposium. He serves as a reviewer of the IEEE TRANSACTIONS ON ANTENNAS AND PROPAGATION, IEEE ACCESS, *Communications in Computational Physics*, IEEE ANTENNAS AND WIRELESS PROPAGATION LETTERS, IEEE MICROWAVE AND WIRELESS COMPONENTS LETTERS, *IET Radar, Sonar & Navigation*, and *Applied Computational Electromagnetic Society Journal*.

Pan Pan Wang was born in Shangqiu, Henan, China. She received the B.S. degree from the Zhengzhou University of Light Industry, Henan, China, in 2015. She is currently pursuing the M.S. degree at Xidian University, Xi'an, Shaanxi, China.

Her current research interests include multiphysics simulation and computational electromagnetics (EMs).

Li Jun Jiang (Fellow, IEEE) received the B.S. degree in electrical engineering from the Beijing University of Aeronautics and Astronautics, Beijing, China, in 1993, the M.S. degree from Tsinghua University, Beijing, in 1996, and the Ph.D. degree from the University of Illinois at Urbana-Champaign, Champaign, IL, USA, in 2004.

From 1996 to 1999, he was an Application Engineer with Hewlett-Packard Company. Since 2004, he has been a Post-Doctoral Researcher, a Research Staff Member, and a Senior Engineer at IBM Thomas J. Watson Research Center, Yorktown Heights, NY, USA. Since the end of 2009, he has been an Associate Professor with the Department of Electrical and Electronic Engineering, The University of Hong Kong, Hong Kong. From September 2014 to March 2015, he was also a Visiting Scholar at the University of California at Los Angeles, Los Angeles, CA, USA. His research interests focus on electromagnetics (EMs), computational electromagnetics, IC signal/power integrity, IC EMC/EMI, antennas, and multiphysics modeling.

Dr. Jiang is an IEEE AP-S Member, an IEEE MTT-S Member, an ACES Member, and a member of the Chinese Computational Electromagnetics Society. In 1998, he received the HP STAR Award. In 2003, he received the IEEE MTT Graduate Fellowship Award and the Y.T. Lo Outstanding Research Award in 2004. In 2008, he received the IBM Research Technical Achievement Award. He was the Semiconductor Research Cooperation (SRC) Industrial Liaison for several academic projects. He has been a TPC Member of IEEE Electrical Design for Advanced Packaging and Systems (EDAPS) since 2010, a TPC member of 2013 IEEE International Conference on Microwave Technology & Computational Electromagnetics (ICMTCE), a Scientific Committee Member of 2010 Workshop on Simulation and Modeling of Emerging Electronics (SMEE), a Special Session Organizer of IEEE EDAPS, the International Review of Progress in Applied Computational Electromagnetics (ACES), Asia-Pacific Radio Science Conference (AP-RASC), a Co-Organizer of HKU Computational Science and Engineering Workshops from 2010 to 2012, a TC-9 and TC-10 Member of IEEE EMC-S since 2011, the TPC Chair of the 7th International Conference on Nanophotonics (ICNP), the TPC Member of the 3rd Conference on Advances in Optoelectronics and Micro/Nano Optics (AOM), the Co-Chair of International Workshop on Pulsed Electromagnetic Field at the Delft, The Netherlands, in 2013, the Chair of 14th IEEE Hong Kong AP/MTT Postgraduate Conference, and the session chairs of many international conferences. He is an Associate Editor of IEEE TRANSACTIONS ON ANTENNAS AND PROPAGATION, an Editor of *Progress in Electromagnetics Research*, and an Associate Guest Editor of the *Proceedings of the IEEE* Special Issue from 2011 to 2012. He also serves as a reviewer of IEEE TRANSACTIONS on several topics and other primary electromagnetics and microwave-related journals.

Wei E. I. Sha (Senior Member, IEEE) received the B.S. and Ph.D. degrees in electronic engineering from Anhui University, Hefei, China, in 2003 and 2008, respectively.

From July 2008 to July 2017, he was a Post-Doctoral Research Fellow and then a Research Assistant Professor with the Department of Electrical and Electronic Engineering, The University of Hong Kong, Hong Kong. From March 2018 to March 2019, he worked at University College London, London, U.K., as a Marie-Curie Individual Fellow. In October 2017, he joined the College of Information Science and Electronic Engineering, Zhejiang University, Hangzhou, China, where he is currently a tenure-tracked Assistant Professor. His research involves fundamental and applied aspects in computational and applied electromagnetics (EMs), nonlinear and quantum electromagnetics, micro- and nano-optics, optoelectronic device simulation, and multiphysics modeling. He has authored or coauthored 170 refereed journal articles, 140 conference publications, eight book chapters, and two books. His Google Scholar citation is 7060 with H-index of 42. His research interests include theoretical and computational research in electromagnetics and optics, focusing on the multiphysics and interdisciplinary research.

Dr. Sha is a member of OSA. He served as a reviewer for 60 technical journals and a technical program committee member of ten IEEE conferences. In 2015, he was awarded the Second Prize of Science and Technology from Anhui Province Government, China. He also received six Best Student Paper prizes and one Young Scientist Award with his students. He also served as an Associate Editor of IEEE JOURNAL ON MULTISCALE AND MULTIPHYSICS COMPUTATIONAL TECHNIQUES, IEEE OPEN JOURNAL OF ANTENNAS AND PROPAGATION, and IEEE ACCESS.

Mei Song Tong (Senior Member, IEEE) received the B.S. and M.S. degrees in electrical engineering from the Huazhong University of Science and Technology, Wuhan, China, in 1985 and 1988, respectively, and the Ph.D. degree in electrical engineering from Arizona State University, Tempe, AZ, USA, in 2004.

He is currently a Distinguished Professor and the Head of the Department of Electronic Science and Technology and the Vice Dean of the College of Microelectronics, Tongji University, Shanghai, China. He has also held an adjunct professorship at the University of Illinois at Urbana-Champaign, Urbana, IL, USA, and an honorary professorship at The University of Hong Kong, Hong Kong. He has published more than 400 papers in refereed journals articles and conference proceedings and coauthored six books or book chapters. His research interests include electromagnetic (EM) field theory, antenna theory and design, simulation and design of RF and microwave circuits and devices, interconnect and packaging analysis, inverse electromagnetic scattering for imaging, and computational electromagnetics.

Prof. Tong is a Fellow of the Electromagnetics Academy and the Japan Society for the Promotion of Science (JSPS) and a Full Member (Commission B) of the USNC/URSI. He has been the Chair of Shanghai Chapter (since 2014) and SIGHT committee (2018) in IEEE Antennas and Propagation Society. He was a recipient of the Visiting Professorship Award from Kyoto University, Japan, in 2012, and from The University of Hong Kong, Hong Kong, 2013. He advised and coauthored six papers that received the Best Student Paper Award from different international conferences. He was a recipient of the Travel Fellowship Award of USNC/URSI for the 31th General Assembly and Scientific Symposium (GASS) in 2014, the Advance Award of Science and Technology of Shanghai Municipal Government in 2015, the Fellowship Award of JSPS in 2016, and the Innovation Award of Universities' Achievements of Ministry of Education of China in 2017. He also frequently served as the session organizer/chair, the technical program committee member/chair, and the general chair for some prestigious international conferences. He has served as an Associate Editor or a Guest Editor for several well-known international journals, including *IEEE Antennas and Propagation Magazine*, IEEE TRANSACTIONS ON ANTENNAS AND PROPAGATION, IEEE TRANSACTIONS ON COMPONENTS, PACKAGING AND MANUFACTURING TECHNOLOGY, *International Journal of Numerical Modelling: Electronic Networks, Devices and Fields*, *Progress in Electromagnetics Research*, and *Journal of Electromagnetic Waves and Applications*. In 2018, he was selected as a Distinguished Lecturer (DL) of IEEE Antennas and Propagation Society for 2019–2021.

Ying Liu (Senior Member, IEEE) received the M.S. and Ph.D. degrees in electromagnetics (EMs) from Xidian University, Xi'an, China, in 2001 and 2004, respectively.

From 2006 to 2007, she carried on post-doctoral research with Hanyang University, Seoul, South Korea. She is a currently a Full Professor and the Leader of the National Key Laboratory of Antennas and Microwave Technology, Xidian University. She has authored or coauthored over 100 refereed journal articles. She has also authored the *Prediction and Reduction of Antenna Radar Cross Section* (Xidian University Press, 2010) and the *Antennas for Mobile Communication Systems* (Electronics Industry Press, 2011). Her research interests include prediction and control of antenna RCS as well as antenna theory and technology.

Dr. Liu is a Fellow of the IET and the Chinese Institute of Electronics (CIE). She was a recipient of "New Century Excellent Talents in University" of the Ministry of Education for China in 2011. She is the Chair of the IEEE AP Xi'an Chapter. She is a reviewer for several international journals and serves as the TPC co-chair for several IEEE flagship conferences.

Wei Jun Wu was born in Hubei, China, in 1985. He received the B.S. degree in information administration and information system and the Ph.D. degree in electromagnetic (EM) fields and microwave technology from Xidian University, Xi'an, China, in 2007 and 2012, respectively.

He works as a Senior Engineer with the Science and Technology on Electromagnetic Compatibility Laboratory, China Ship Development and Design Center, Wuhan, China. His current research interests include filtering antenna, antenna arrays, and EMC.

Guang Ming Shi (Fellow, IEEE) received the B.S. degree in automatic control, the M.S. degree in computer control, and the Ph.D. degree in electronic information technology from Xidian University, Xi'an, China, in 1985, 1988, and 2002, respectively.

He joined the School of Electronic Engineering, Xidian University, in 1988. From 1994 to 1996, as a Research Assistant, he cooperated with the Department of Electronic Engineering, The University of Hong Kong, Hong Kong. Since 2003, he has been a Professor with the School of Electronic Engineering, Xidian University, and the Head of the National Instruction Base of Electrician and Electronic (NIBEE) in 2004. From June 2004 to December 2004, he had studied at the Department of Electronic Engineering, University of Illinois at Urbana-Champaign (UIUC), Urbana, IL, USA. He is currently the Vice President of Xidian University. He has authored or coauthored over 60 research articles. His research interests include compressed sensing, theory and design of multirate filter banks, image denoising, low bit rate image/video coding, and implementation of algorithms for intelligent signal processing (using DSP and FPGA).